MODELLING GAS FLOW EXPERIMENTS IN MX80 BENTONITE: ANALYSIS OF PREFERENTIAL GAS PATHS

I.P. Damians[*], S. Olivella[*], and A. Gens[*]

[*] Department of Civil and Environmental Engineering
Universitat Politècnica de Catalunya – BarcelonaTech (UPC)
Campus Nord UPC, 08034 Barcelona, Spain
Email: ivan.puig@upc.edu

Key words: Hydro-Mechanical 3D model, Gas flow, Mx80 bentonite

Abstract. *A gas injection test, performed on compact bentonite, was carried out at the British Geological Survey. The test is composed by two stages (i.e. hydration followed by gas injection testing). After gas breakthrough and a period of gas flow through the sample, the injection pump was stopped whilst the stresses and porewater pressures were continuously monitored. A Hydro-Mechanical 3D numerical model has been developed to simulate the gas injection test and to achieve similar gas pressure, gas outflow, and stress evolution responses.*

1 INTRODUCTION: MX80-D TEST

A gas injection test performed on compacted Mx80 bentonite was carried out at the British Geological Survey. This experiment, designated as Mx80-D, represents the first test dataset for a series of tests analyzed by DECOVALEX Task A [1]. These tests are useful to increase the understanding of gas flow potential trough this low permeability materials.

Figure 1a presents the testing cell apparatus with some outer instrumentation details. Figure 1b presents the model of the bentonite sample (dimensions: 12 cm-length × 6 cm-diameter) including injection and backpressure porous stone filters, the model mesh discretization by layers definition, and the external volumes related to the linked radial array sensors.

The Mx80-D test is composed by two main stages: hydration stage followed by helium gas injection. The injected gas pressure was fixed to 1 MPa from 7.3 to 39.3 days and 3 MPa from 39.4 to 46 days according to test duration. After that, gas flow rate was continuously increased at the injection from 0 to 8.0×10^{-7} kg/s/m^2 (from 46 to 67 days) and then maintained constant (i.e., flow rate value of 8.0×10^{-7} kg/s/m^2) until a breakthrough point occurred (i.e., at 71.5 days). After breakthrough and a period of gas flow through the sample, the injection pump was stopped whilst the stresses and porewater pressures were continuously monitored at several sample control point locations up to the end of the test at day 121.

2 MATERIAL PROPERTIES, NUMERICAL MODEL, BOUNDARY CONDITIONS

The problem was modelled accordingly with gas flow rate previously detailed. Table 1 presents the material properties and some details of the constitutive equations of the embedded fracture model assumed. Figure 2 presents the random porosity strategy assumed at each model sample layer, and Figure 3 presents the intrinsic permeability trends obtained as a function of the strains development according to the random permeability weighting distribution assumed (see Table 1 – Note-a) returning an initial equivalent global permeability of 3.3×10^{-21} m^2 (which was a problem input). Elastic modulus of 307 MPa and Poisson's ratio of 0.4 were considered.

a) b)

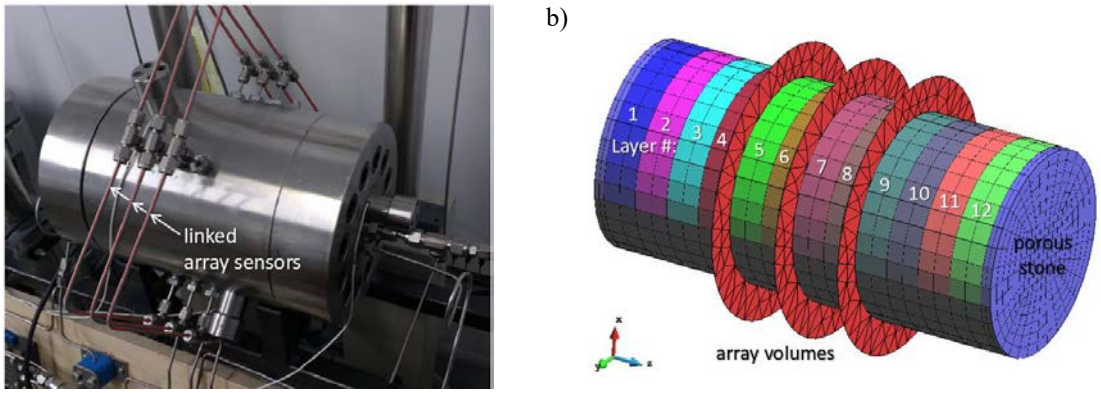

Figure 1: Mx80-D test: pressure vessel and arrays (a) and inner Mx80 sample model mesh detail (b).

Table 1: Material model parameters for the Mx80 bentonite:

Initial porosity	Intrinsic permeability (a)	Water retention curve (b)		Relative permeability (c)	Embedded fractures definition parameters (a-d)			
		P_0	λ		a	b_0	b_{max}	ε_0
0.44	1.0×10^{-19}	10.8	0.45	$n_l = 3$,	5.0×10^{-4}	9.5×10^{-9}	7.5×10^{-7}	0.01
	1.0×10^{-20}	22.5		$n_{g,matrix} = 2$,	5.0×10^{-5}	5.0×10^{-9}	3.5×10^{-7}	0.03
	1.0×10^{-21}	48.6		$n_{g,fractures} = 1$	5.0×10^{-6}	1.5×10^{-9}	1.5×10^{-7}	0.05
-	m^2	MPa	-	n-power				

Notes: (a) Initial matrix random intrinsic permeability according to 1/6-weighting distribution for 1×10^{-19} m^2 and 1×19^{-20} m^2, and 2/3-weighting distribution for 1×10^{-21} m^2 (see Figure 2). The global intrinsic permeability is defined as a function of material matrix and internal fracture permeabilities: $k_{ii} = k_{matrix} + k_{fractures}$ (see Note-d below);
(b) Water retention curve according to Van Genuchten model (λ: shape function);
(c) Liquid and gas relative permeability defined by the effective saturation: $k_r = (S)^n$, where S is the degree of saturation;
(d) Definition parameters of the embedded fractures related to the associated width of the fractures (a), fracture apertures (b_0 and b_{max}), and strain development (ε and ε_0).

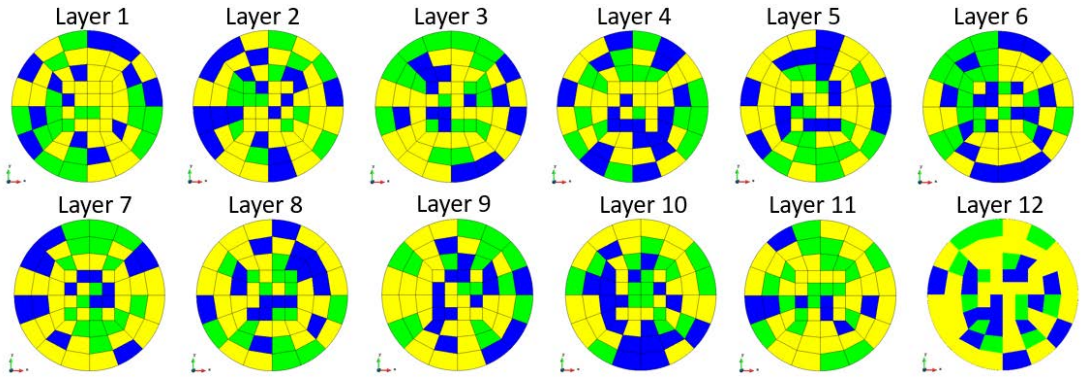

Figure 2: Layer-by-layer random permeability distribution (with different weighting) for the not-connected case: Green: $k_0 = 1\times10^{-19}$ m^2 (1/6 weighting), blue: $k_0 = 1\times19^{-20}$ m^2 (1/6 weighting), and yellow: $k_0 = 1\times10^{-21}$ m^2 (2/3 weighting). Note: Layer 11th was the one selected for the connected permeability case, randomly rotated and distributed along sample's axial axis)

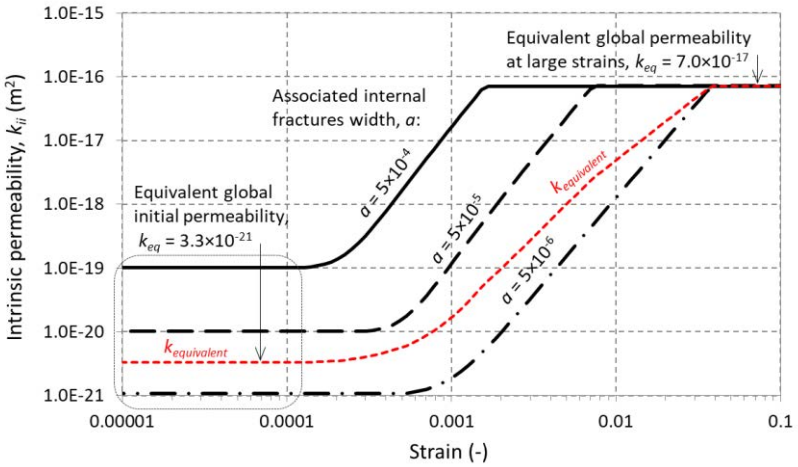

Figure 3. Intrinsic permeability evolution related/equivalent global permeability representation (generated by weighted geometric mean).

Two alternative preferential path strategies of permeability distribution were performed:

a) Not-connected permeability case: Random distribution of three different permeabilities through all model layers (2/3 weighting to the lowest permeability zone and 1/6 weighting to the middle and higher permeability zones; see Figure 2).
b) Connected permeability case: Random distribution of the three different permeabilities specified in a selected/representative layer (Layer 11th as per Figure 2), which was then randomly rotated to both directions to define the other sample layers, generating a sort of connectivity along the axial axis of the sample.

3 RESULTS

Figure 4 presents the injection gas pressure and backpressure outflow evolution results for both not-connected and connected permeability cases. Despite better agreement was obtained for the not-connected permeability case if the dissipation trend of the gas pressure is analysed, much better agreement was obtained in terms of the gas pressure peak-value and outflow magnitude for the connected permeability case. Figure 5 shows the advective gas flux (m^3/m^2/s) vectors for both cases of connectivity during injection at day 65 (just before the breakthrough) and at day 95 (during gas dissipation). The same scale (vectors size factor) is maintained to ease the comparison. As expected, different location of the larger flow-vector magnitudes take place before and after the breakthrough. Also, as it can be noticed, the vectors appeared more addressed in the connected permeability case than in the not connected case due to the less connectivity between elements. In addition to the injection gas pressure, also radial porewater at three different locations was obtained. As it can be observed in Figure 6, reasonably well agreement was achieved for the connectivity cases analysed. Also here, the peak and first dissipation trending shape was better approximated by the connected case (Fig.6b) whereas the long-term dissipation trending shape was probably better fitted by the not-connected case (Fig.6a). Figure 7 presents the evolution of both axial and radial stresses evolution during the test. As it can be seen, both connectivity cases returned reasonably well agreement with the measured data, with a good approximation of the ranging values due to the gas breakthrough jump despite the smoother increasing trend obtained by both the model calculations.

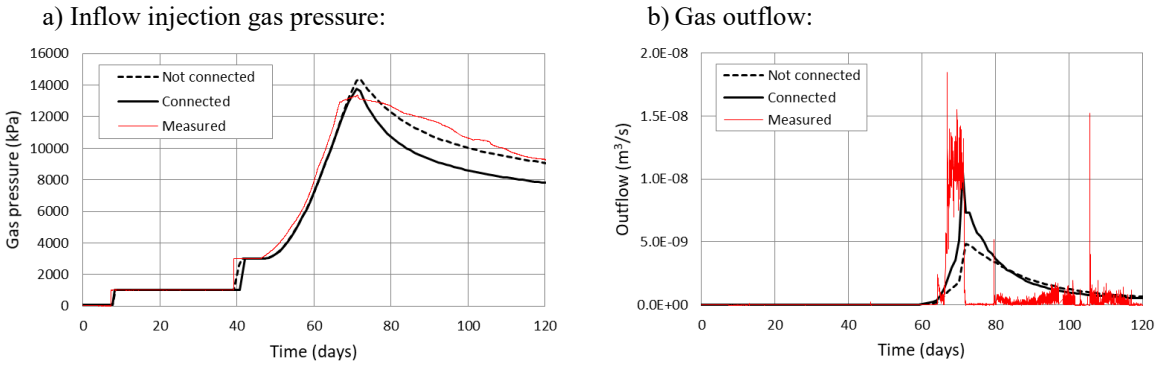

Figure 4: Injection gas pressure (a) and gas outflow (b) evolution.

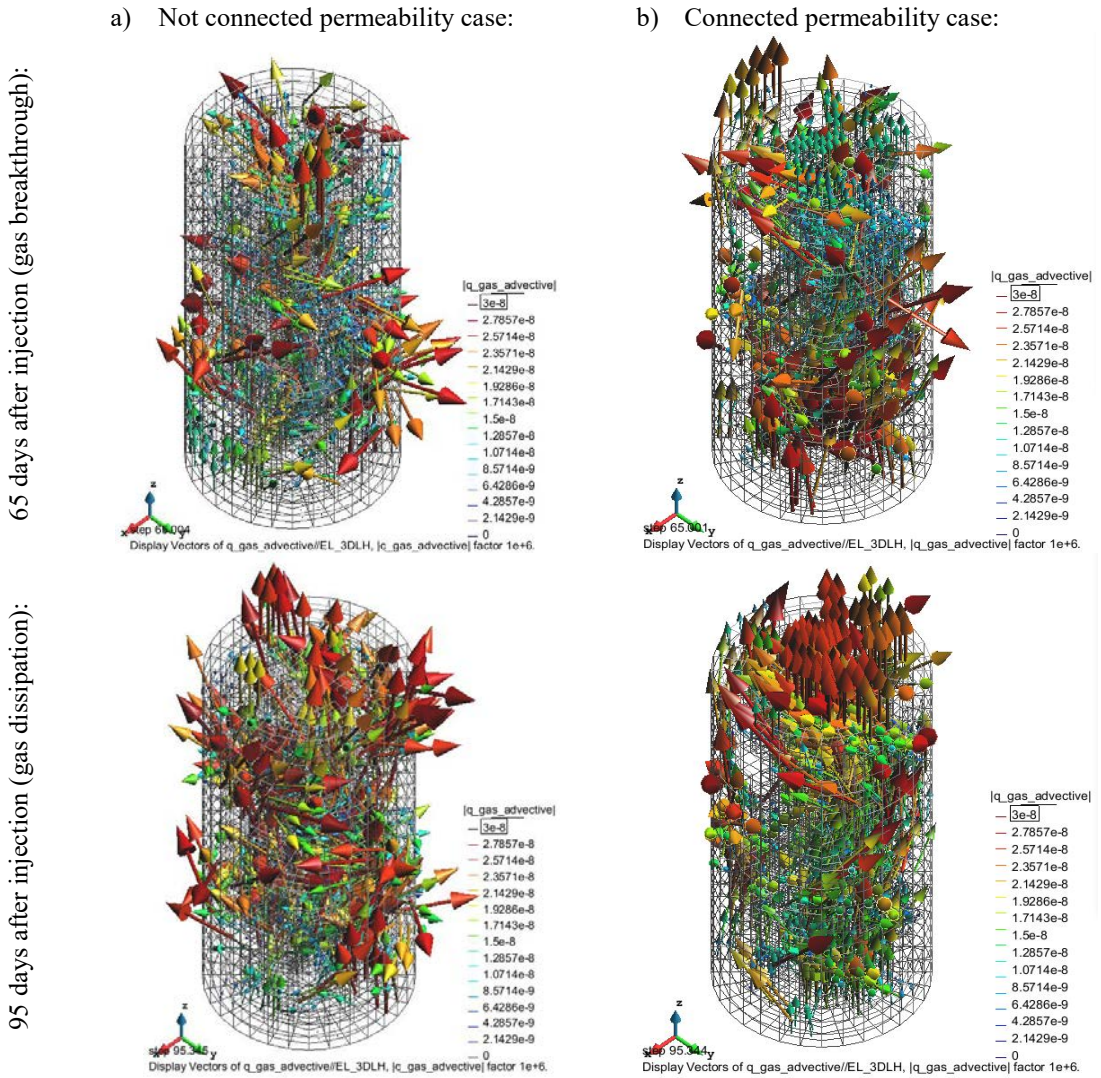

Figure 5: Advective gas flux at day 65 (a: gas breakthrough) and at day 95 (b: gas dissipation).

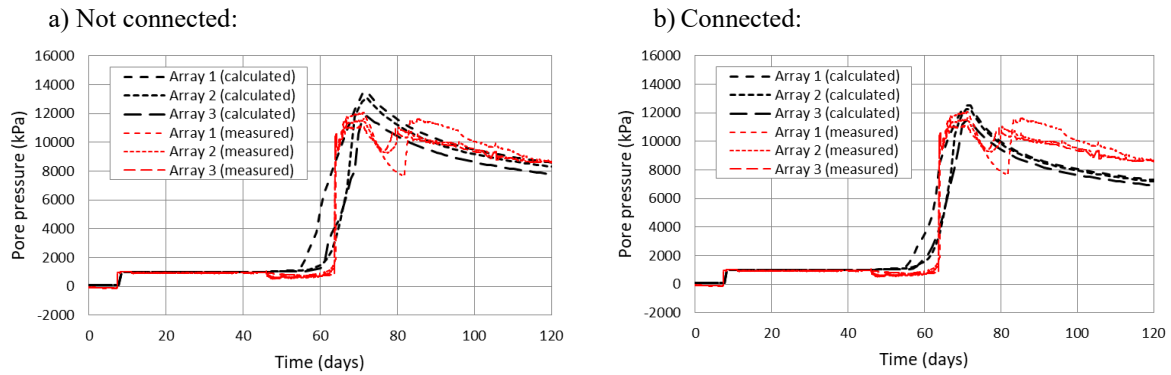

Figure 6: Gas pressure evolution at arrays: not connected (a) and connected (b) permeability cases.

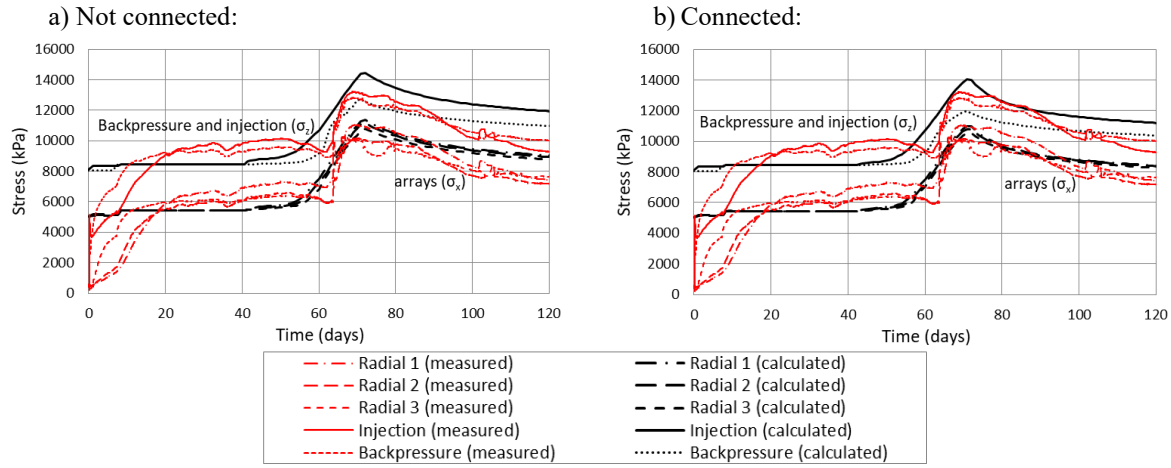

Figure 7: Axial and radial stress evolution: not connected (a) and connected (b) permeability cases.

4 CONCLUSIONS

- It has been possible to incorporate the mechanical effect on the previous just hydraulic 3D model, in addition to the soil permeability based on embedded discontinuities (which in turn depends on deformation).
- The proposed methodology for the preferential paths analyses provides results reasonably satisfactory for both connectivity cases assumed.

ACKNOWLEDGEMENTS

Study supported by the National Radioactive Waste Management Agency (ANDRA).

REFERENCES

[1] Harrington, J, R Cuss, C Graham, S, British Geological Survey, Radioactive Waste Management Limited, ENGINEER (modElliNg Gas INjection ExpERiments), DECOVALEX 2019, Specifications for Task A.